

# The influence of the spin-flip transitions on the photon spectrum from ultra-relativistic electrons in the field of a crystal.

Andrei V. Korol<sup>†‡ ¶</sup>, Andrey V. Solov'yov<sup>†§ +</sup>, and Walter Greiner<sup>† \*</sup>

<sup>†</sup>Institut für Theoretische Physik der Johann Wolfgang Goethe-Universität, 60054 Frankfurt am Main, Germany

<sup>‡</sup>Department of Physics, St.Petersburg State Maritime Technical University, Leninskii prospect 101, St. Petersburg 198262, Russia

<sup>§</sup>A.F.Ioffe Physical-Technical Institute of the Academy of Sciences of Russia, Polytechnicheskaya 26, St. Petersburg 194021, Russia

**Abstract.** We investigate the influence of the spin-flip transitions on formation of the spectral distribution of the radiation emitted by ultra-relativistic of tens to hundreds GeV electrons incident along crystallographic axis in a thin single crystal. Both the formalism and the numerical data are presented. The calculated spectra for 35 to 243 GeV electrons in W crystal are compared with the dependences obtained experimentally [1].

## 1. Introduction

The aim of this paper is to carry out quantitative analysis of the role of the spin-flip transitions in formation of the total emission spectra by ultra-relativistic electrons which traverse single crystal close to its axial direction. This study was stimulated by a recent paper [1] where the experimental data on radiative energy loss of  $\varepsilon = 35$  to 243 GeV electrons incident on a W single crystal are presented and, to a great extent, are interpreted as the first experimental evidence of a significant contribution of spin to the radiative spectrum.

The photon emission by a highly relativistic particle in a static field of crystalline axis/plane and the magnetic bremsstrahlung (or synchrotron radiation) are examples of the radiative processes occurring in strong fields. It is a well-established fact (e.g.

¶ E-mail: korol@th.physik.uni-frankfurt.de, korol@rpro.ioffe.rssi.ru

+ E-mail: solovyov@th.physik.uni-frankfurt.de, solovyov@rpro.ioffe.rssi.ru

\* E-mail: greiner@th.physik.uni-frankfurt.de

[2, 3]) that quantum effects start manifesting themselves in the photon spectrum when a dimensionless quantum parameter  $\chi$  exceeds the value of  $\approx 0.1$ . The quantum parameter can be written as  $\chi = \gamma H/H_0$  (for magnetic bremsstrahlung) or  $\chi = \gamma E/E_0$  (for the radiation process in the external electric field), where  $\gamma = \varepsilon/mc^2$  is the relativistic factor of projectile,  $H/E$  is the strength of the magnetic/electric field and  $H_0 = E_0 = m^2c^3/e\hbar$  is the critical field.

In this paper we focus attention on the influence of the spin-related effects on the formation of the spectral distribution of unpolarized photons emitted by tens to hundreds GeV electrons incident under small angle  $\vartheta_0$  to crystallographic axes of a thin single crystal.

Theoretical approaches suitable for the analysis of the influence of the spin-related effects on the radiative spectrum of ultra-relativistic particles in a strong external field include (a) the quasi-classical method based on the operator representation of the projectile's wave function [4, 5] (see also [6]), (b) the approach based on the correspondence principle and utilizing the equivalent photon method [7] (see also [8]), (c) the full quantum-electrodynamical treatment of a kinetic equation for an electron moving in the field of a crystal axis [9].

In section 2 we present general formulae which allow to estimate quantitatively the contribution of the spin-flip transitions to the total radiative spectrum. This part of the paper, which is included to make the reading easier, contains all the essential expressions which were used to carry out the numerical analysis. They represent the quasi-classical formalism described in great detail in [5].

To say it very clearly: (a) All the formulae are from [5] except one (equation (9) below) which could not be found there. This refers to the explicit expression for the differential intensity with spin-flip. (b) In application to the radiation emission in crystals the formulae contain the standard CFA (constant field approximation) and correction terms (for details see section 2). (c) When carrying out the numerical analysis we used both methods, 'pure CFA' and 'CFA + corrections'.

The numerical results are presented, discussed and compared with the experimental data [1] in section 3. A summary of the results and possible directions for further improvement of the theoretical model are given in section 4.

## 2. The formalism

Within the framework of the quasi-classical approach the spectral-angular distribution of the energy radiated by an ultra-relativistic particle (of a spin  $s = 1/2$ ) moving in an external static field is given by the following formulae

$$\frac{dE(\vec{\xi}, \vec{\xi}')}{\hbar d\omega d\Omega_{\mathbf{n}}} = \alpha \frac{\omega^2}{4\pi^2} \int dt_1 \int dt_2 R(t_2, t_1; \vec{\xi}, \vec{\xi}') e^{i\omega' \Phi(t_2, t_1)} \quad (1)$$

$$R(t_2, t_1; \vec{\xi}, \vec{\xi}') = \frac{1}{4} \text{Sp} \left[ \left(1 + \vec{\xi} \cdot \vec{\sigma}\right) (A^*(t_2) - i\vec{\sigma} \cdot \mathbf{B}^*(t_2)) \left(1 + \vec{\xi}' \cdot \vec{\sigma}\right) (A(t_1) + i\vec{\sigma} \cdot \mathbf{B}(t_1)) \right] \quad (2)$$

$$\Phi(t_2, t_1) = t_1 - t_2 - \frac{1}{c} \mathbf{n} \cdot ((\mathbf{r}(t_1) - \mathbf{r}(t_2))) \quad (3)$$

$$A(t) = \frac{c \mathbf{e}^* \cdot \mathbf{p}(t)}{2 \sqrt{\varepsilon \varepsilon'}} \left[ \left( \frac{\varepsilon' + mc^2}{\varepsilon + mc^2} \right)^{1/2} + \left( \frac{\varepsilon + mc^2}{\varepsilon' + mc^2} \right)^{1/2} \right] \quad (4)$$

$$\mathbf{B}(t) = \frac{c \mathbf{e}^*}{2 \sqrt{\varepsilon \varepsilon'}} \cdot \left[ \left( \frac{\varepsilon' + mc^2}{\varepsilon + mc^2} \right)^{1/2} \mathbf{p}(t) - \left( \frac{\varepsilon + mc^2}{\varepsilon' + mc^2} \right)^{1/2} (\mathbf{p}(t) - \hbar \mathbf{k}) \right] \quad (5)$$

The notations used are as follows:  $\alpha$  is the fine structure constant,  $\omega$ ,  $\mathbf{k}$  and  $\mathbf{e}$  are, respectively, the photon energy, wave vector and polarization vector,  $\mathbf{n} = c \mathbf{k} / \omega$  denotes the direction of the emission,  $c$  is the light velocity,  $d\Omega_{\mathbf{n}}$  is the solid angle associated with  $\mathbf{n}$ . The initial and final energies of the projectile are denoted by  $\varepsilon$  and  $\varepsilon' = \varepsilon - \hbar\omega$ , the quantities  $\vec{\xi}$  and  $\vec{\xi}'$  stand for the polarization vectors of the initial and final states respectively,  $\vec{\sigma}$  is the vector constructed from the Pauli matrices  $\sigma_j$  ( $j = x, y, z$ ). The quantity  $\omega'$  is defined as  $\omega' = \omega(\varepsilon/\varepsilon')$

The remarkable feature of the quasi-classical formulae (1-5) is that they combine the classical description of the projectile's dynamics and the specific quantum effects. Indeed, the integrand in (1) is time-dependent through the functions  $\mathbf{p}(t)$  and  $\mathbf{r}(t)$  which represent the classically defined momentum and the position vector of the projectile moving in an external field. Therefore the emitted radiation is described in terms of the trajectory defined by  $\mathbf{p}(t)$  and  $\mathbf{r}(t)$ , as in classical electrodynamics; it is uniquely parametrized by the initial energy  $\varepsilon$  and the initial values  $\mathbf{p}_0 = \mathbf{p}(0)$  and  $\mathbf{r}_0 = \mathbf{r}(0)$ . On the other hand, these expressions account for two important types of quantum corrections: (a) the radiative recoil (i.e. the change in the projectile energy/momenta due to photon emission) which formally enters the integrand in (1) through the 'corrected' photon frequency  $\omega'$ , and (b) the dependence of the intensity of radiation on the spin quantum numbers of the projectile. The latter enter the formulae through the two-component polarization density matrices  $(1 + \vec{\xi} \cdot \vec{\sigma})/2$  and  $(1 + \vec{\xi}' \cdot \vec{\sigma})/2$  (see (2)).

The quantum corrections related to the projectile's dynamics in the external field are neglected. This is fully justified provided the particle can be considered as an ultra-relativistic in both the initial and the final states. Hence, it is implied that the relativistic factors satisfy the strong inequalities  $\gamma = \varepsilon/mc^2 \gg 1$ ,  $\gamma' = \varepsilon'/mc^2 \gg 1$ . If these conditions are met then, as it is proved in [4, 5] (see also the recent paper [6]), the expressions (1-5) can be used to evaluate the characteristics of radiation emitted by a projectile moving in an arbitrary static field.

Once the functions  $\mathbf{p}(t)$  and  $\mathbf{r}(t)$  are known, then these formulae allow one to evaluate the most detailed characteristics of the emitted radiation. These include

the dependence of  $dE$  not only on the photon energy and the emission angle but the polarizational properties as well. In particular, one can analyze the role of the spin degree of freedom in the radiative process.

To obtain expressions describing the radiative spectra of a collimated bunch of unpolarized electrons passing through a crystal close to the axial direction one has to carry out the following transformation of the right-hand side of (1): (a) summation over the photon polarizations, (b) averaging over the electron polarizations (the cases  $\xi' = \pm\xi$  have to be considered separately), (c) integration over the emission angles, and (d) averaging over the fast oscillatory transverse motion of the electrons due to the action of the axial field. The transformations (a)-(c) are carried out using standard methods (see, e.g., [2, 5]). An adequate approach for averaging over the transverse motion is based on the statistical description of the particle distribution in the phase space ([5, 10]). In a thin crystal, where one can neglect the influence of multiple scattering from the crystal nuclei and electrons, the differential probability,  $dw$ , for a projectile with (transverse) coordinate  $\vec{\rho}$  and velocity  $\mathbf{v}_\perp$  can be written as follows

$$dw(\vec{\rho}, \mathbf{v}_\perp) = \frac{d^2\vec{\rho}}{s} F(\vec{\rho}, \vartheta_0), \quad (6)$$

where  $s$  is the area corresponding to one axis, and  $\vartheta_0$  is the incident angle with respect to the axis (see the illustrative figure 1).<sup>7</sup> The distribution function  $F(\vec{\rho}, \vartheta_0)$  is defined

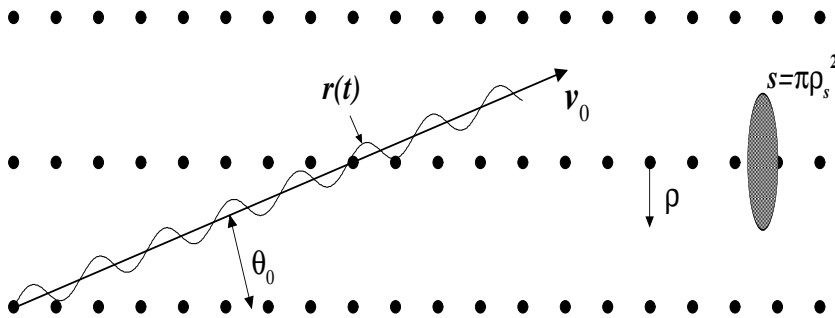


**Figure 1.** Schematic representation of the passage of an ultra-relativistic particle through an oriented crystal. Under the action of the crystalline field  $U$  (the filled circles denote the positions of atomic nuclei arranged into the crystallographic axes, - atomic strings) the trajectory  $\mathbf{r}(t)$  of the particle varies along the direction of the vector  $\mathbf{v}_0$ , which is the mean velocity. The picture corresponds to the case when incident angle  $\vartheta_0$  exceeds the Lindhard's angle  $\vartheta_L$ . The dashed ellipse denotes the area,  $s = \pi\rho_s^2$ , allocated for one axis. The field of each atomic string is supposed to be axially symmetric within  $s$ :  $U = U(\rho)$  where  $\rho$  is the distance from the axis.

by the initial conditions at the entrance. In the case of an axially symmetric potential

$U(\rho)$  of the atomic string the function  $F(\vec{\rho}, \vartheta_0) \equiv F(\rho, \vartheta_0)$  is given by:

$$F(\rho, \vartheta_0) = \int \frac{d^2 \vec{\rho}_0}{s(\varepsilon_{\perp 0})} \theta(\varepsilon_{\perp 0} - U(\rho)), \quad (7)$$

where  $s(\varepsilon_{\perp 0}) = \int d^2 \vec{\rho} \theta(\varepsilon_{\perp 0} - U(\rho))$  is the allowed area for the transverse motion in a unit cell,  $\theta(x)$  is the Heaviside function:  $\theta(x) = 1$  when  $x > 0$ , and  $\theta(x) = 0$  if otherwise. The quantity  $\varepsilon_{\perp 0}$  stands for the transverse energy  $\varepsilon_{\perp 0} = \varepsilon \vartheta_0^2/2 + U(\rho_0)$  which, for given  $\vartheta_0$  and the entrance coordinate  $\rho_0$ , is the constant of motion in a thin crystal. Note that for the incident angles larger than the critical Lindhard-angle,  $\vartheta_L = (2U_0/\varepsilon)^{1/2}$  (where  $U_0$  is the depth of the potential well), when  $\varepsilon_{\perp 0} > U_0$ , the right-hand side of (7) reduces to unity.

Carrying out all the operations mentioned above one obtains the spectral distributions of the emitted energy (per path  $dl = c dt$ ) in the following form:

$$\left\langle \frac{dE^{(t)}}{\hbar d\omega dl} \right\rangle = \frac{1}{\pi \rho_s^2} \int_0^{2\pi} d\varphi_{\vec{\rho}} \int_0^{\rho_s} \rho d\rho F(\rho, \vartheta_0) \overline{\frac{dE^{(t)}}{\hbar d\omega dl}}, \quad (8)$$

where the brackets designate the averaging over the phase space, and the bars indicate that the averaging over the initial polarizations of the projectile is carried out. The integration is carried out over the area allocated for one axis,  $s = \pi \rho_s^2$ , where  $\rho_s$  is half the distance between two neighbouring axes of the same type.

The superscript '(t)' specifies the type of the spectral distribution: (t) = ( $\pm$ ) correspond to the spectra with, (-), and without, (+), the spin-flip transitions, and (t) = (tot) designates the total spectrum which is the sum of the (+)- and (-)-terms.

The spectral distribution appearing in the integrand of (8) reads

$$\overline{\frac{dE^{(t)}}{\hbar d\omega dl}} = \frac{\alpha}{\lambda_c \gamma} C^{(t)} \frac{i}{2\pi} \int_{-\infty}^{\infty} \frac{d\tau}{\tau + i0} e^{i\Phi(\tau)} \left(1 + \beta^{(t)} A(\tau)\right), \quad (9)$$

where  $\lambda_c$  is the Compton wavelength of the electron. For the cases '(t)=(tot)' and '(t)=(-)' the coefficients  $C^{(t)}$  and  $\beta^{(t)}$  are given in terms of the fractional photon energy  $\mu = \hbar\omega/\varepsilon$ ,  $0 \leq \mu \leq 1$ :

$$C^{(\text{tot})} = -\mu, \quad C^{(-)} = \frac{\mu^3}{6(1-\mu)}, \quad \beta^{(\text{tot})} = 1 - \mu + \frac{1}{1-\mu}, \quad \beta^{(-)} = -2. \quad (10)$$

For small incident angles  $\vartheta_0$  one can use the continuous model for the potential of the axis. Then, assuming this potential to be axially symmetric, solving (approximately) the equation of motion  $\dot{\mathbf{v}}(t) = \varepsilon^{-1} (dU(\rho)/d\vec{\rho})$  using on the right-hand side the relation  $\mathbf{r}(t) = \mathbf{r}_0 + \mathbf{v}_0 t$  for the position vector ( $\mathbf{v}_0$  is the the mean velocity of the particle), and, finally, using the obtained expressions in eqs. (1)-(5), one finds that the functions  $\Phi(\tau)$  and  $A(\tau)$  can be represented as follows

$$\Phi(\tau) = \frac{\omega' \tau}{\gamma^2} \left[ 1 + \frac{\vartheta_v^2}{\pi^2} \int d^2 \mathbf{q} d^2 \mathbf{q}' \frac{\mathbf{q} \cdot \mathbf{q}'}{q_0 q'_0} e^{i(\mathbf{q} + \mathbf{q}') \cdot \vec{\rho}} e^{-\frac{u^2}{2}(q^2 + q'^2)} W(q) W(q') \right]$$

$$\times \left( \frac{\sin(q_0 + q'_0)\tau}{(q_0 + q'_0)\tau} - \frac{\sin(q_0\tau)\sin(q'_0\tau)}{q_0\tau q'_0\tau} \right), \quad (11)$$

$$A(\tau) = -\frac{\vartheta_v^2}{\pi^2} \int d^2\mathbf{q} d^2\mathbf{q}' \frac{\mathbf{q} \cdot \mathbf{q}'}{q_0 q'_0} e^{i(\mathbf{q}+\mathbf{q}')\vec{\rho}} e^{-\frac{u_t^2}{2}(q^2+q'^2)} W(q) W(q') \sin(q_0\tau) \sin(q'_0\tau), \quad (12)$$

where  $\vartheta_v = U_0/mc^2$ ,  $W(q)$  is the atomic formfactor,  $u_t$  is the amplitude of thermal vibrations of the atoms, and  $q_0 = \mathbf{q} \cdot \mathbf{v}_0$ . The integration is carried out over the vectors  $\mathbf{q}$  and  $\mathbf{q}'$  lying in the plane perpendicular to the axis. The details of derivation of eq. (9) in the case of the total spectrum can be found in [5].

Let us note here that the radiative transitions accompanied by the spin-flip process manifest themselves for large energies of the emitted photon,  $\hbar\omega \sim \varepsilon$ . Indeed, it follows from (9-10) that  $\overline{dE^{(-)}} \propto \mu^3/(1-\mu)$ . The latter quantity is negligibly small for  $\mu \ll 1$  and increases as  $\mu \sim 1$ . It is known (see, e.g. [2, 5]) that the emission of such energetic quanta becomes noticeable in the radiative spectrum when the quantum parameter  $\chi_s$  becomes large,  $\chi_s > 1$ . Hence, the magnitude of  $\chi_s$  defines the effective range of the emitted photon energies. In the case of an ultra-relativistic particle passing through a crystal close to the direction of a crystallographic axis the parameter  $\chi_s$  is conveniently represented in the following form:

$$\chi_s = \gamma \frac{\lambda_c}{a_s} \frac{U_0}{mc^2}. \quad (13)$$

The quantity  $a_s$  represents the effective screening radius of the potential created by a string of the crystal atoms. For the potential of (111) axis in a tungsten crystal, where  $U_0 \approx 400$  eV,  $a_s \approx 0.2$  Å (see, e.g. [5]), it follows that  $\chi_s = 1$  is achieved for the incident electron energy 35 GeV. Hence, one can expect that the effects due to the spin-flip transitions will manifest themselves in the total radiative spectrum of an  $\varepsilon > 35$  GeV electron moving at small angle  $\vartheta_0$  with respect to (111) direction in a W crystal.

From the computational viewpoint the direct calculation of the functions (11-12) and, correspondingly, the spectra (9) is a non-trivial problem even if one utilizes simple analytic forms for the axial potential such as the Molière approximation or the Lindhard potential [10]. Considerable simplification of the formulae is achieved within a so-called constant field approximation (CFA) [5]. The latter implies that the change in the particle's radial distance,  $\Delta\rho = v_\perp \tau_c = c\vartheta_0 \tau_c$ , occurring during the time interval  $\tau_c = l_c/c$  (here  $l_c \sim c\gamma^2/\omega'$  is a coherence length), is smaller than the typical scale  $a_s$  within which the axial field changes noticeably. Hence, provided the condition  $l_c\vartheta_0 < a_s$  is met, one can expand the integrands in (11-12) in powers of  $q_0\tau \sim c\vartheta_0\tau/a_s < 1$ . If, in addition, the incident angle  $\vartheta_0$  is small compared with  $\vartheta_v$ , then the terms proportional to  $(\vartheta_0/\vartheta_v)^2$  can be treated as small corrections. Within this approximation the functions (11-12) are expressed in terms of local characteristics of the trajectory. The final result,

valid for both the total spectrum and for its part due to the spin-flip, reads

$$\frac{\overline{dE^{(t)}}}{\hbar d\omega dl} = \frac{\alpha C^{(t)}}{\lambda_c \gamma} \left\{ \int_z^\infty \text{Ai}(\xi) d\xi + \beta^{(t)} \frac{\text{Ai}'(z)}{z} - \frac{\vartheta_0^2}{\vartheta_v^2} \left[ \beta^{(t)} (aF_1(z) - bF_2(z)) + bF_3(z) \right] \right\} \quad (14)$$

where  $\text{Ai}(\cdot)$  and  $\text{Ai}'(\cdot)$  are the Airy function and its derivative respectively (see, e.g., [11]). Other variables and functions are defined as follows:

$$z = \left( \frac{u}{\chi(\rho)} \right)^{2/3}, \quad u = \frac{\mu}{1 - \mu}, \quad (15)$$

$$\chi(\rho) = \chi_s w'(y), \quad (16)$$

$$y = \frac{\rho}{a_s}, \quad w(y) = \frac{U(\rho)}{U_0}, \quad (17)$$

$$a = \frac{1}{3} \frac{2h_1 + h_2}{y^4 g^2}, \quad b = \frac{1}{15} \frac{2h_1 + h_2 + h_3}{y^4 g^2}, \quad (18)$$

$$h_1 = \frac{yg'}{g}, \quad h_2 = y \frac{w''' - 3g'}{2g}, \quad h_3 = \frac{1 + (1 + h_1)^2}{6}, \quad g = \frac{w'}{y}, \quad (19)$$

$$F_1(z) = \frac{z\text{Ai}'(z) + \text{Ai}(z)}{z^2}, \quad F_2(z) = \frac{6z\text{Ai}'(z) + (4 + z^3)\text{Ai}(z)}{z^2},$$

$$F_3(z) = \frac{2z\text{Ai}'(z) + z^3\text{Ai}(z)}{z^2}. \quad (20)$$

By expressing  $\text{Ai}(z)$  and  $\text{Ai}'(z)$  in terms of the modified Bessel functions  $K_{1/3}(x)$  and  $K_{2/3}(x)$  with  $x = 2z^{3/2}/3$  (see, e.g., [11]) we reproduce the formula presented in §17 of [5].

The first two terms on the right-hand side of (14) are independent of the incident angle  $\theta_0$  and represent the quasi-classical spectral distribution of the radiated energy in the magnetic bremsstrahlung limit (see, e.g. [2, 5]).

The last three terms on the right-hand side of (14) represent the correction to the CFA due to the change in the field strength on the scale of the coherence length,  $l_c$ . These terms appear as a result of the transformation of a more general expression (9). The range of validity of (14) is subject to two conditions: (a)  $\vartheta_0 \ll \vartheta_v$ , and (b)  $l_c \vartheta_0 < a_s$ .

### 3. Numerical results

In this section we present the results of calculations of the spectral intensity of radiation emitted by ultra-relativistic electrons in the energy range  $\varepsilon = 35 - 243$  GeV incident with  $\vartheta_0 = 0.3$  mrad from (111) axis in a W crystal of a thickness 0.2 mm. The parameters correspond to those used in a recent experiment [1] where the main emphasis was put on the investigation of the role of the spin-flip process in forming the total radiative spectrum.

The calculation of the spectral intensity was based on the formulae (14-20). The averaging over the projectile trajectories was carried out according to the rule (8) where we used  $F(\rho, \vartheta_0) = 1$  which is justified by the relation  $\vartheta_0 > \vartheta_L$ . Indeed, for the potential of a (111) axis the depth of the potential well is  $\approx 1000$  eV and, therefore, the Lindhard critical angle  $\vartheta_L = 0.09 \dots 0.2$  mrad for  $\varepsilon = 35 - 243$  GeV.

We used a continuous potential approximation for modelling the field of an atomic string. The potential of an individual atom was calculated by using the radial wavefunctions within the non-relativistic Hartree-Fock approximation. For the distances  $\rho = [0, \rho_s]$  (where  $\rho_s = L_c/\sqrt{6}$  is the half-distance between two (111) axes,  $L_c = 3.165$  Å is the lattice constant of a W crystal [12]) the potential of the individual string was corrected by accounting for the potentials created by the nearest six axes. Only axially-symmetric part of the resulting field was used. The dependence of the field strength  $dU(\rho)/d\rho$  on the distance  $\rho$  from the axis are plotted in figure 2. The screening distances,  $a_s$ , defined as the root of the equation  $dU(a_s)/d\rho = e^{-1} (dU/d\rho)_{max}$ , are equal to 0.125 Å for the crystal temperature  $T = 70$  K and to 0.191 Å for  $T = 293$  K.

As functions of  $\rho$  the spectral intensities  $\overline{dE^{(t)}/\hbar d\omega dl}$  depend strongly on the magnitude of the local quantum parameter  $\chi(\rho)$  defined by eq. (16). Namely, the value of  $\chi(\rho)$  defines the effective range of the emitted photon energies. The formal analysis of this statement is as follows. The right-hand side of (14) is expressed in terms of the Airy function and its derivative. These functions satisfy the conditions  $\text{Ai}(z), |\text{Ai}'(z)| = 0.1 \dots 1$  for  $z \leq 1$ , and decrease rapidly (exponentially) as  $z$  goes beyond 1. The same is valid for the integral term,  $\int_z^\infty \text{Ai}(\xi) d\xi$  (see, e.g., [11]). Hence, in the  $\rho$ -range where  $\chi(\rho) \ll 1$ , the spectral distributions increases sharply within the interval of low energies of the emitted photon,  $\hbar\omega = 0 \dots \hbar\omega_{max}$  with  $\hbar\omega_{max} \approx \chi(\rho)\varepsilon \ll \varepsilon$ , and decrease rapidly as  $\hbar\omega/\varepsilon > \chi(\rho)$ . If  $\chi(\rho) \gg 1$  then the condition  $z \sim 1$  produces (see (15))  $\hbar\omega_{max}/\varepsilon \sim 1$  which makes possible the emission of energetic quanta. In this case the total spectral distribution  $\overline{dE^{(tot)}/\hbar d\omega dl}$  is (roughly) flat within the interval  $\hbar\omega/\varepsilon = 0 \dots 1$  [5]. The contribution of the spin-flip term becomes noticeable (and comparable in magnitude with the total spectrum) at the hard end of the spectrum whereas for  $\hbar\omega/\varepsilon \ll 1$  it is negligibly small. The latter result immediately follows if one compares the coefficients  $C^{(tot)}$  and  $C^{(-)}$  (see (10)): for  $\mu \ll 1$  the following strong inequality is valid  $C^{(-)}/C^{(tot)} \approx \mu^2 \ll 1$ .

Figures 3(a-b) represent the dependences  $\chi(\rho)$  for two temperatures of the crystal and for different energies of the projectile (as specified). For the sake of comparison the values of the quantum parameter  $\chi_s$  (see (13)) are plotted as well. The maximum distance  $\rho_s$  is defined by the crystal symmetry and the chosen crystallographic direction and is independent on the crystal temperature. For a (111) axis in a W crystal  $\rho_s = 1.292$  Å. As mentioned above the shape of the spectral distribution (14) is quite sensitive to the magnitude of the local quantum parameter  $\chi(\rho)$ . The range  $\tilde{\rho}_1 < \rho < \tilde{\rho}_2$  (where

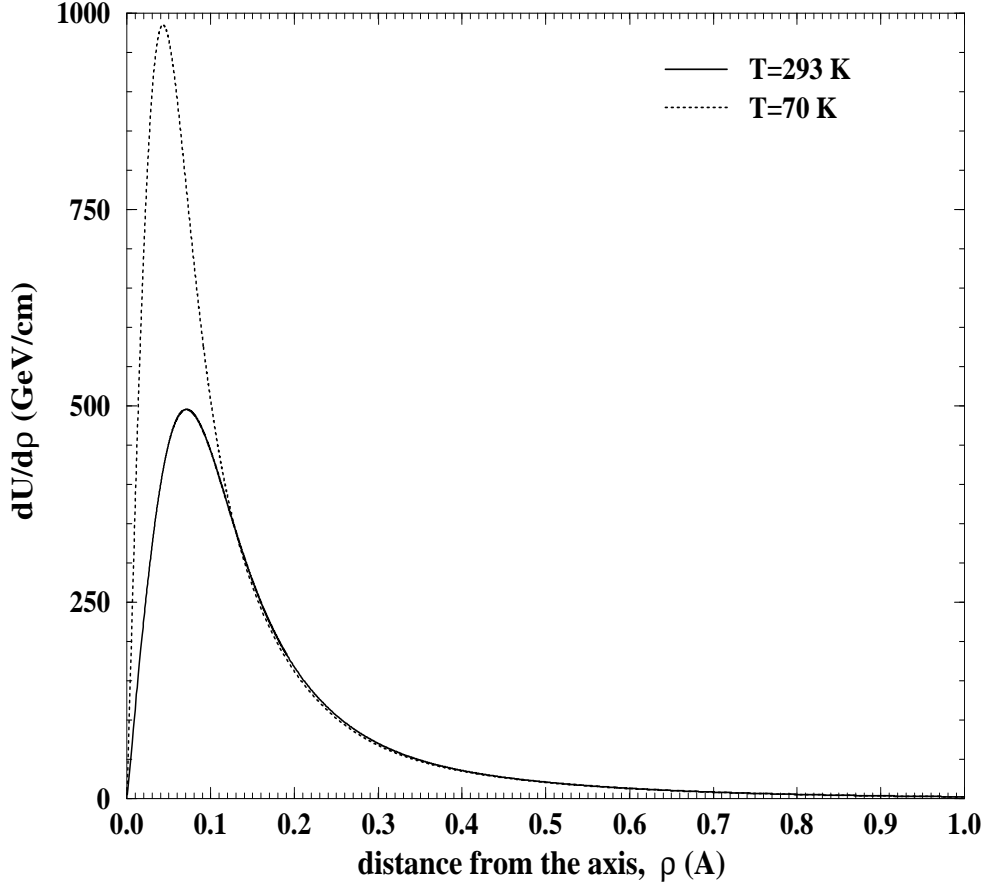


**Figure 2.** The field strength,  $dU(\rho)/d\rho$ , of a (111) axis in W as a function of the distance from the axis for two different temperatures as indicated.

$\tilde{\rho}_{1,2}$  are the roots of the equation  $\chi(\rho) = 1$  establishes, for given temperature and energy, the distances from the axis which contribute effectively to the emission of high energy photons ( $\hbar\omega \sim \varepsilon$ ) and, consequently, define the fraction of spectrum due to the spin-flip transitions. For fixed temperature the values of  $\tilde{\rho}_{1,2}$  do not depend on  $\varepsilon$ , while the interval  $[\tilde{\rho}_1, \tilde{\rho}_2]$  increases with  $T$ . Thus, the intervals of the radial distances which contribute to the spin-flip part of the total spectrum ranges from  $\approx [0.05, 0.18]$  Å for  $T = 70$  K to  $\approx [0.0, 0.44]$  Å for  $T = 293$  K. Comparing these values with the range  $\rho \leq \rho_s = 1.292$ , one can anticipate that the radiative spectrum *averaged* over the whole interval of the radial distances (see (8)) is influenced, to a great extent, by the contribution of the regions where  $\chi(\rho) < 1$ . As a result, even for high energies of the projectile electron the relative yield of soft photons is larger than that of  $\hbar\omega \sim \varepsilon$ .

Keeping in mind the large variation in the values of the local quantum parameter

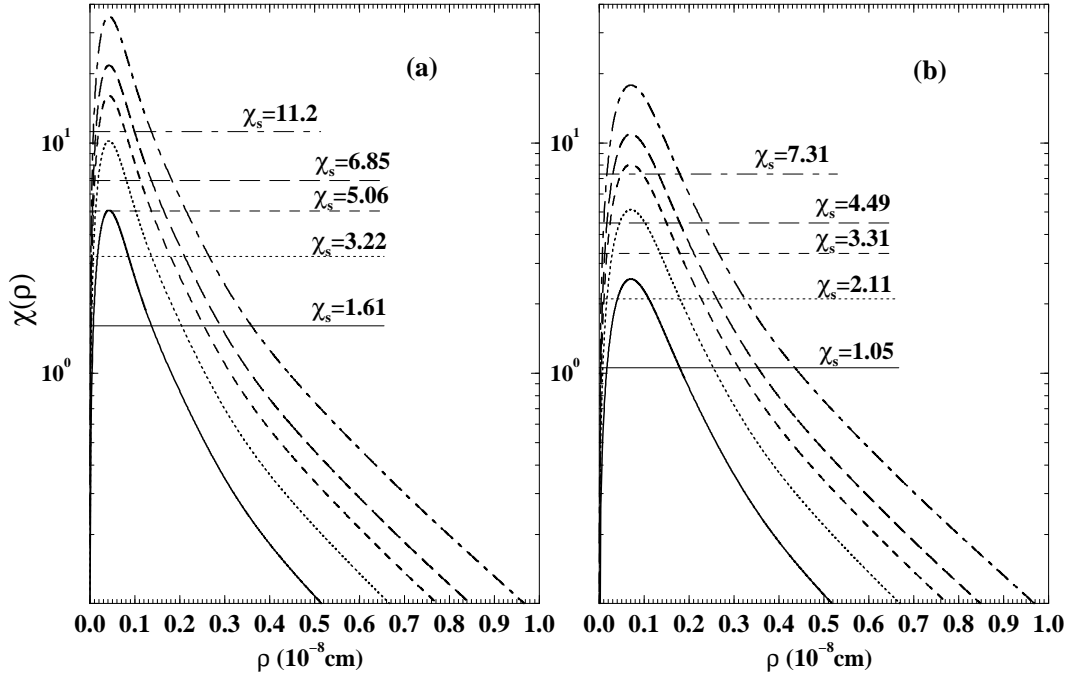


**Figure 3.** The local quantum parameter  $\chi(\rho)$  (see (16)) versus the distance from the axis  $\rho$  for the field of (111) axis in W calculated for  $T = 70$  (figure (a)) and for  $T = 293$  K (figure (b)), and for different incident energies:  $\varepsilon = 35$  GeV (solid lines),  $\varepsilon = 70$  GeV (dotted lines),  $\varepsilon = 110$  GeV (dashed lines),  $\varepsilon = 149$  GeV (long-dashed lines),  $\varepsilon = 243$  GeV (dot-dashed lines). The horizontal lines mark the corresponding magnitudes of  $\chi_s$ .

within the interval  $\rho \leq \rho_s$  of the accessible distances ( $\chi(\rho)$  is of the order  $10^{-3}$  for  $\rho \approx \rho_s$ , - this range is not presented in figures 3(a-b)), it becomes clear that to obtain realistic estimates of the spectral distribution of radiation one has to carry out the proper averaging procedure.

The results of our calculations of the radiative spectra are presented in figures 4 (a-e). The energies of electrons as well as the incident geometry (as specified in the caption) correspond to the experimental conditions [1]. In addition to the information presented in the caption let us note the following. The averaging procedure was carried out according to (8) where we used  $F(\rho, \vartheta_0) = 1$  which is adequate for the over-barrier motion in a thin crystal. Thus, we have disregarded the evolution of the distribution function due to the effects of multiple scattering and the radiation damping. All curves in figures 4 (a-e) were obtained within the CFA, i.e. by using the first two terms in the curly brackets on the right-hand side of (14). The dependences represented by open circles were calculated (at  $T = 293$  K) using a more elaborated method. For the photon

frequencies satisfying the condition  $l_c \vartheta_0 < a_s$  we used (14) including the correction terms proportional to  $\vartheta_0^2/\vartheta_v^2$ . To calculate the total radiative spectrum in the region of lower photon energies we made use of the asymptotic expressions (17.11-12) from [5] which are valid, within logarithmic accuracy, for  $\chi_s \gg 1$  and  $\mu > \chi_s (a_s/\rho_s)^{3/2}$ .

For the sake of comparison in figure 4(f) we plotted the spectral distributions calculated for a  $\varepsilon = 243$  GeV electron and for the incident geometry as described above but *without* averaging over the radial distances  $\rho$ . The curves corresponding to  $T = 70$  and 293 K were obtained by accounting for the first two terms in (14) where the constant values of the quantum parameter  $\chi = \chi_s$  (see figure 3) were used. It is exactly this approximation which was used, as one understands, in [1] when interpreting the experimental data.

First we discuss the differences between the averaged and non-averaged intensities. There are three features which clearly distinguish the curves in figure 4 (f) from their analogies in figure 4 (e). These are: (a) the absolute magnitude of the intensities, (b) the shapes of the spectral distributions, and (c) the differences between the  $T = 70$  K and  $T = 243$  K spectra.

Although striking, these differences can be easily understood. To illustrate this let us analyze the behaviour of the intensities due to the spin-flip transitions. The analysis of the discrepancies in the total spectral distributions can be carried out using similar arguments.

It is easily checked that for large values of  $\chi_s$  the corresponding non-averaged spectral intensity due to the spin-flip transition attains its maximum at the photon energies satisfying the condition  $u = \mu/(1 - \mu) \approx \chi_s$ . A quantitative estimate of the intensity in the vicinity of the maximum reads

$$\left( \frac{dE^{(-)}}{\hbar d\omega dl} \right)_{\substack{\chi=\chi_s \\ u\approx\chi_s}} \approx -\frac{\alpha}{3\lambda_c\gamma} \chi_s \text{Ai}'(1), \quad (21)$$

where  $\text{Ai}'(1) \approx -0.16$ .

To estimate the magnitude of the averaged intensity in the photon energy range  $u \approx \chi_s$  one first notices that the principal contribution comes from the spatial region where the local quantum parameter  $\chi(\rho)$  is greater than  $\chi_s$  (see figure 3). Denoting the roots of the equation  $\chi(\rho) = \chi_s$  through  $\rho_{1,2}$ , and taking into account that  $\rho_1^2 \ll \rho_2^2$  one obtains the following estimate:

$$\left\langle \frac{dE^{(-)}}{\hbar d\omega dl} \right\rangle_{u\approx\chi_s} \approx -\frac{\alpha}{3\lambda_c\gamma} \chi_s \int_{\rho_1}^{\rho_2} \frac{2\rho d\rho}{\rho_s^2} \frac{\text{Ai}'(z)}{z} \approx -\frac{\alpha}{3\lambda_c\gamma} \eta \langle \chi \rangle \langle z \rangle^{1/2} \text{Ai}'(\langle z \rangle), \quad (22)$$

where  $\langle \chi \rangle$  is the average value of the quantum parameter over the region  $\rho_1 \leq \rho \leq \rho_2$ . For the temperatures 70 and 293 K  $\langle \chi \rangle$  equals to 21.1 and 12.3, respectively. The quantity  $\langle z \rangle$ , defined as  $\langle z \rangle = (\chi_s/\langle \chi \rangle)^{2/3}$ , equals 0.65 for  $T = 70$  K and 0.71 for  $T = 293$

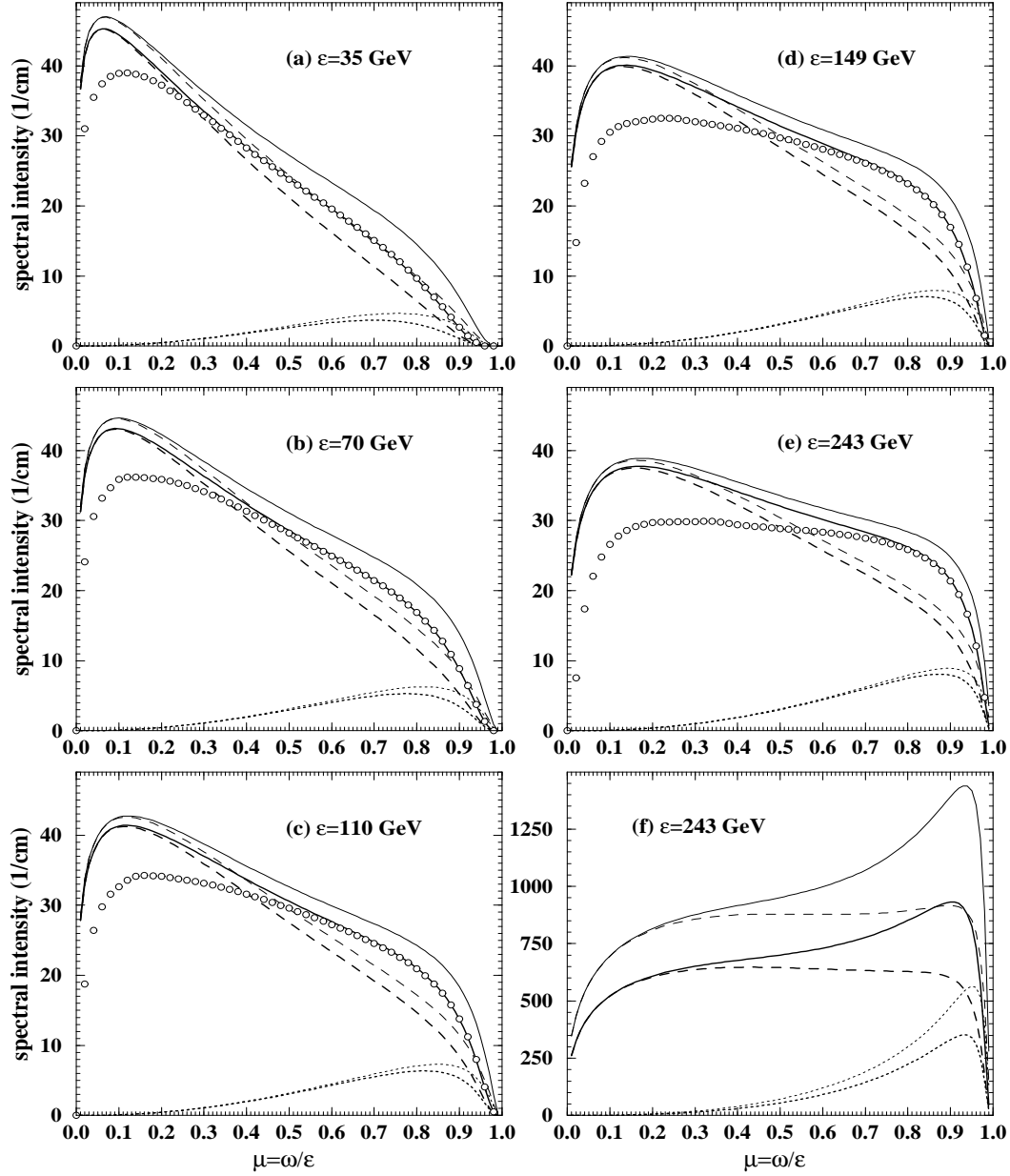


**Figure 4.** In figures (a-e): the averaged spectral distributions of radiation (see (8)) calculated for different energies of electrons (as indicated) aligned 0.3 mrad from the (111) axis in W. Thick lines refer to the crystal temperature 293 K, thin lines correspond to  $T = 70$  K. Solid lines and open circles represent the dependences of the total intensity, dotted lines stand for the contribution of the spin-flip transitions, dashed lines reflect  $\langle dE^{(+)} / \hbar d\omega dl \rangle$ . See also explanations in the text. Figure (f) shows the spectral distributions of radiation from a  $\epsilon = 243$  GeV electron in W at  $T = 70$  and 243 K calculated without the averaging over the  $\rho$ -interval and for fixed values of the quantum parameter,  $\chi = \chi_s$ . The legend is as in figures (a-e).

K. One easily checks (see, e.g., [11]) that for both of these values  $\langle z \rangle^{1/2} \text{Ai}'(\langle z \rangle) \approx -0.167$ . The parameter  $\eta$  stands for the ratio  $\rho_2^2/\rho_s^2$  yielding the values  $\eta \approx 0.012$  for  $T = 70$  K and  $\eta \approx 0.019$  for  $T = 293$  K. The factor  $\chi_{eff} \equiv \eta \langle \chi \rangle$  represents by itself the effective quantum parameter which defines the absolute magnitude of the averaged intensity in the range of the photon frequencies  $\hbar\omega \sim \varepsilon$ .

The right-hand sides of eqs. (21) and (22), reproducing with a reasonable accuracy the maximum values of the spectral intensities due to the spin-flip transition (the dotted curves in figures 4 (e) and (f)), allows one to explain the discrepancies between the averaged and non-averaged spectra. The excess of the non-averaged intensities over the averaged ones is reproduced by the ratio  $\chi_s/\chi_{eff}$  which equals 44 at  $T = 70$  K and 31 at  $T = 293$  K which are close to the exact values which follow from figures 4 (e) and (f): 57 and 43, respectively. The different behaviour of the two types of the spectral distributions also follows from the above written formulae. Indeed, the ratio  $\chi_s(T = 70)/\chi_s(T = 293) = 1.7$  explains the difference between the thick and thin dotted lines in figures 4 (e), whereas the ratio  $\chi_{eff}(T = 70)/\chi_{eff}(T = 293) \approx 1.1$  illustrates that the averaged intensities are much less sensitive to the change in the crystal temperature.

The behaviour of  $\overline{\langle dE^{(tot)}/\hbar d\omega dl \rangle}$ , represented by solid lines in figures 4 (a-e), illustrates the known tendencies of the total spectral distributions obtained within the CFA [5]. Namely, for comparatively low incident energies, when the local quantum parameter is small in a wide interval of the distances (see figure 3) the spectrum has maximum at  $\hbar\omega \ll \varepsilon$  and decreases rapidly with the photon energy. As  $\varepsilon$  increases, the range where  $\chi(\rho) \gg 1$  increases as well giving rise to the yield of the photons with  $\hbar\omega \sim \varepsilon$ . The magnitude of the intensity in the low- $\omega$  region decreases and the spectrum becomes flatter over the whole range of photon energies.

Similar features characterize the total spectral distributions obtained from (8) and (14) including the correction terms proportional to  $\vartheta_0^2/\vartheta_v^2 \approx 0.16$ , - the open circles in figures 4 (a-e). The contribution of the correction terms is negligibly small for  $\hbar\omega \sim \varepsilon$  when the coherence length is small enough so that the characteristics of the spectrum are defined by the instant value of the particle's acceleration. Their influence becomes visible in the low-energy part of the spectrum. As it is seen, the inclusion of the correction terms decreases the magnitude of the spectrum for  $\hbar\omega \ll \varepsilon$  which leads to a further flattening of the distribution.

Commenting on the spectral intensities due to the spin-flip transitions we note the following. For all incident energies the spectra become pronounced close to the tip-region. This feature, which is known for both the synchrotron radiation [2, 3, 4] and for the radiation by electrons in the field of crystals [1, 5, 7, 8], can be easily traced from the general formulae (9-10). Indeed, the spin-flip intensity is proportional to the factor  $\mu^3/(1 - \mu)$  which is small for  $\mu \ll 1$  and increases as  $\mu \sim 1$ . For  $\mu \rightarrow 1$  the spectrum

$\overline{dE^{(-)}/\hbar d\omega dl}$  exponentially decreases due to the highly oscillatory exponential factor in the integrand in (9). The contribution to the averaged spectrum (8) comes from the spatial region where  $\chi(\rho) \gg 1$ . The position of the maximum of  $\langle \overline{dE^{(-)}/\hbar d\omega dl} \rangle$  can be estimated as  $\mu \approx 1 - \langle \chi \rangle^{-1}$ , see (22). The latter formula, as it is mentioned above, allows to estimate the magnitude of the maximum intensity, which is almost independent of  $\gamma$  for sufficiently high energy of the electron. Indeed, apart from the explicit factor in the denominator, the dependence on  $\gamma$  enters the right-hand side of (22) through  $\langle \chi \rangle$  and  $\langle z \rangle$ . Since the ratio  $\langle \chi \rangle / \gamma$  is independent of the relativistic factor (see (13) and (16)), the dependence in question is concentrated in  $\langle z \rangle^{1/2} \text{Ai}'(\langle z \rangle)$  which is a slowly increasing function of  $\gamma$ . This feature is clearly seen in the figures: the maximum of  $\langle \overline{dE^{(-)}/\hbar d\omega dl} \rangle$  increases by a factor of 2 with the energy variation from 35 to 243 GeV.

Let us mention that the spin-flip spectral distributions were obtained within the CFA, omitting the correction terms on the right-hand side of (14). These terms contribute noticeably to the region  $\mu \ll 1$  but are negligibly small closer to the hard-end of the spectrum.

Finally, let us present the numerical data on the effective radiation length,  $L_{eff}$ . This quantity, which is defined as

$$L_{eff}^{-1} = \int_0^\varepsilon \left\langle \frac{dE^{(tot)}}{d\omega dl} \right\rangle \frac{d\omega}{\varepsilon}, \quad (23)$$

defines the interval within which a particle loses its energy due to the radiation.

The values of  $L_{eff}^{-1}$ , calculated using the averaged CFA spectra with the correction terms included (open circles in the figures), and the ratios  $r = L_{eff}^{-1}/L_{BH}^{-1}$ , where  $L_{BH}^{-1} \approx 4Z^2\alpha r_0^2 n \ln(183Z^{-1/3})$  ( $n$  is the volume density of the crystal atoms,  $r_0$  is the electron classical radius,  $Z$  is the atomic number) is the radiation length due to bremsstrahlung in an amorphous medium, are summarized in table 1. The values of  $r$  are in good agreement with the measured data [1] except for the case  $\varepsilon = 35$  GeV where our result is  $\approx 10\%$  higher.

**Table 1.** The values of  $L_{eff}^{-1}$  (see (23)) and  $r = L_{eff}^{-1}/L_{BH}^{-1}$  calculated for different energies of electron.

$\varepsilon$ (GeV)	35	70	110	149	243
$L_{eff}^{-1}$ (cm $^{-1}$ )	21.50	23.89	25.64	25.77	25.86
$r$	7.10	7.88	8.46	8.51	8.54

In figure 5 we present the results of our calculation together with the experimentally measured spectra [1]. The data refer to the scaled spectral intensity, i.e.  $\langle \overline{dE^{(t)}/\hbar d\omega dl} \rangle$  divided by  $L_{eff}^{-1}$ . The crystal temperature is chosen to be 293 K. It is this  $T$ -value which had been used in the experiment [1] as one can deduce from the paper basing on the

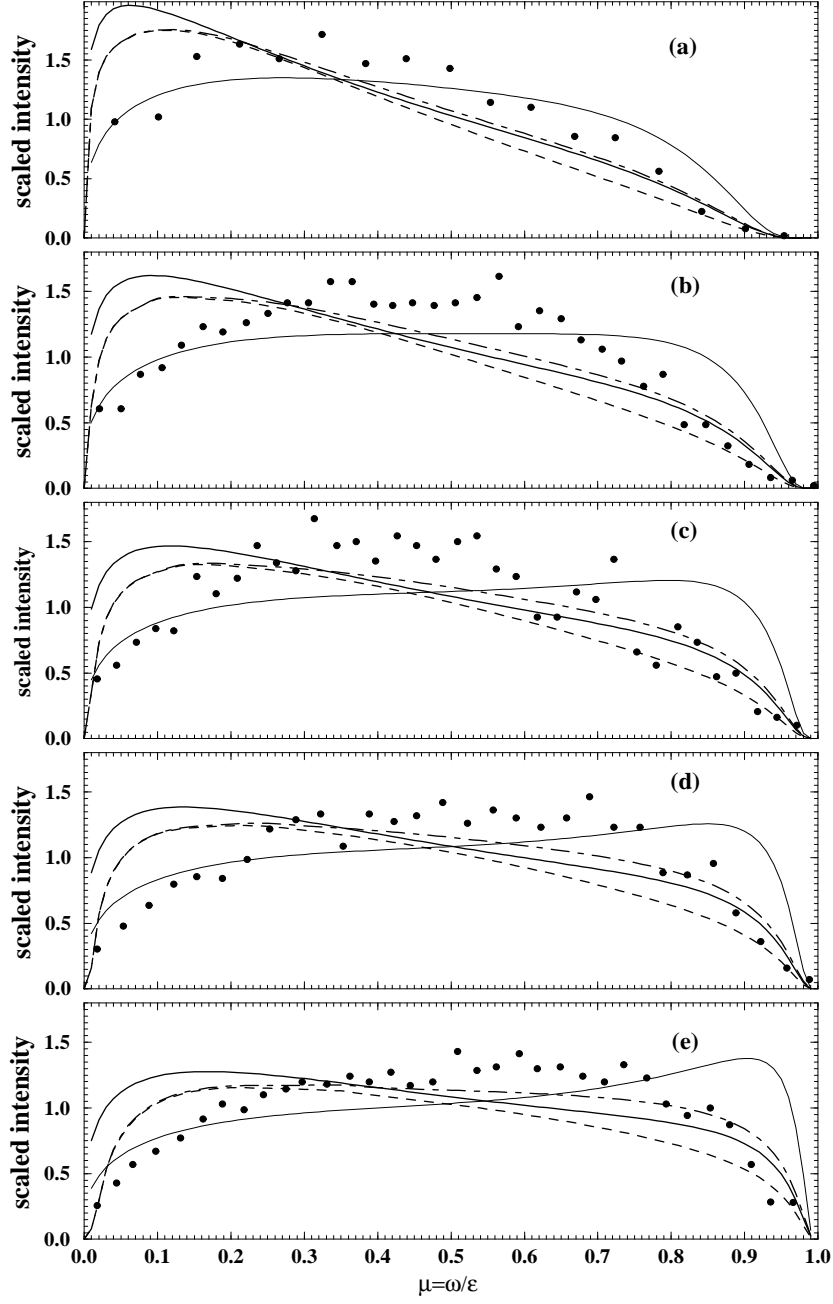


**Figure 5.** Scaled intensities for different incident energies: (a)  $\epsilon = 35$  GeV, (b)  $\epsilon = 70$  GeV, (c)  $\epsilon = 110$  GeV, (d)  $\epsilon = 149$  GeV, (e)  $\epsilon = 243$  GeV. Thick solid lines correspond to the total intensities within CFA. Thick dot-dashed lines represent the total intensities and thick dashed lines stand for the intensities without spin-flip both calculated within the approximation 'CFA + correction terms'. Thin solid lines denote the distributions calculated without the averaging over the  $\rho$ -interval and for fixed values of the quantum parameter,  $\chi = \chi_s$ . All curves correspond to  $T = 293$  K. Full circles are the experimental data [1].

cited values of the parameter  $\chi_s$ . Let us note that we failed to reproduce the curves presented in the cited paper and which, as it follows from the text, correspond to the CFA approximation with constant values  $\chi = \chi_s$  without averaging over the distances  $\rho$  (full lines in figure 1 in [1]). In figure 5 thin lines correspond to the calculation of  $\overline{dE^{(\text{tot})}/\hbar d\omega dl}$  according to (14) but omitting the terms proportional to  $\vartheta_0^2/\vartheta_v^2$  and using the values  $\chi_s$  (as indicated in figure 3(b)) instead of the local parameter  $\chi(\rho)$ . Although it seems like the same approximation is used the shapes of these curves noticeably differs from those presented in the cited paper. In any case this approximation, in our mind, is not adequate to describe the radiative spectra in the crystal (see the discussion in connection with figure 4), so that the thin solid curves are plotted for the illustrative purposes only.

'The scattering of the experimental points indicate the uncertainties' [1]. Taking this into account we may state that for  $\mu > 0.7$  both thick curves, which describe the total intensities, match the experimental data. Note that it is exactly the region where the spin-flip transitions contribute to the total spectrum (see figure 4). In the mid-range of the  $\mu$ -values the computed intensities underestimate the experimental ones, and for  $\mu \ll 1$  theoretical results noticeably overestimate the measured spectra. All these features are typical, as it is seen from the figures, for the whole range of the incident energies, and, in general, the calculated curves are skewed to the left wing of the spectrum as compared to the measured data.

For the sake of comparison we plotted also the scaled intensities of the radiation excluding the contribution of the spin-flip transitions (dashed lines). These were obtained as  $L_{eff} \left( \overline{dE^{(\text{tot})}/\hbar d\omega dl} - \overline{dE^{(-)}/\hbar d\omega dl} \right)$  with both terms in the brackets calculated with the help of (8) and (14), and retaining the correction terms in the latter formula. Taking into account the experimental uncertainties one can observe that these curves taken alone agree fairly well with the measured data on the right wing of the spectrum.

Thus, on the basis of these calculations we cannot confirm in full the statement made in [1] that the region  $\mu \sim 1$  of the radiative spectrum by ultra-relativistic electrons moving under a small incident angle with respect to the crystallographic axis is formed mainly due to the spin-flip transition of the projectile.

#### 4. Concluding remarks

We have calculated the spectral distributions of radiation formed during the passage of multi-GeV unpolarized electrons along (111) axis in W crystal. The consideration was carried out within the framework of the quasi-classical approach [5] which adequately describes the radiative process of ultra-relativistic particles in strong external fields.

Special attention was paid to the investigation of the contribution of the spin-flip

transitions of the projectile to the total spectrum. The results of our study can be summarized as follows. The role of the spin-flip transitions in forming the hard-photon end,  $\hbar\omega \approx \varepsilon$ , of the radiative spectrum is quite noticeable. Definitely, it is much larger than that predicted in [9] where a full quantum-electrodynamical approach was developed. However, we also can hardly agree with the statement made in [1] that it is the spin-flip transitions which do modify dramatically the shape of spectral distributions. The numerical results presented in this paper agree well with the experimental data in the range of photon energies  $\hbar\omega \approx (0.7 \dots 1.0)\varepsilon$ , i.e. exactly where the contribution of the spin-flip transitions becomes pronounced. This fact demonstrates the applicability of the standard CFA model (combined with a proper procedure for averaging over the phase volume of a projectile) for the description of the hard-end of the spectrum for over-barrier particles. For lower photon energies, when the coherence length becomes larger than the typical scale of variation of the potential of a crystallographic axis/plane, it is necessary to go beyond the CFA scheme. In the present paper we utilized the approach suggested in [5] which allows to incorporate the corrections proportional to  $(\vartheta_0/\vartheta_v)^2$ . Our data shows that even when this parameter is small (in the case considered in this paper  $(\vartheta_0/\vartheta_v)^2 = 0.16$ ) the correction terms reduce noticeably the magnitude of the spectral intensity in the range of small photon energies. This approach becomes less adequate as  $\hbar\omega/\varepsilon \ll 1$ . In this case one has to use the formulae (9-12) which include the deviations from the CFA in the most general way.

The theoretical results can be improved further by taking into account three important effects which are intrinsic for the radiative scattering of an ultra-relativistic particle in the field of a crystal. The first one is the analogue of the Landau-Pomeranchuk-Migdal effect [13]. The latter consists in a strong suppression of the yield of the soft-photon bremsstrahlung emitted by an ultra-relativistic particle in medium. This is a result of a number of correlated small-angle collisions of the projectile with the lattice atoms on the scale of the coherence length. Similar effect occurs when the particle moves close to an atomic string in a crystal and under the small angle  $\vartheta_0$  from the axis [14]. The account for this mechanism will reduce the magnitude of the spectral intensity for low photon energies. Another phenomenon to be accounted for is the cascade process of the photon emission which is effectively generated when a multi-GeV electron/positron enters the crystal at small ( $\vartheta_0 < \vartheta_v$ ) angles to the crystallographic axis/plane [5, 15]. The third effect we would like to mention is the influence of the radiative loss on the shape of the emission spectrum. In the present calculations we disregarded the change in the particle's energy on the scale of the crystal thickness  $L$ . However, as soon as  $L$  becomes comparable with the effective radiation length the formalism must include the solution of the proper kinetic equation ([5, 9]). This consideration is fully appropriate in the case considered in the present paper with regard to the experiment [1]. Indeed, the experimental setup included the 0.2 mm

thick W crystal. Comparing this length with the values of  $L_{eff}$  (see table 1) one finds  $L/L_{eff} \approx 0.5$ , so that the electron loses half of its initial energy. Although it is clear, qualitatively, how the radiative loss influences the radiative spectrum (the latter is shifted towards the low-energy part), the rigorous quantitative treatment is to be performed for each specific set of the parameters: the incident energy and the geometry, and the type of the crystal.

Finally, let us mention the phenomenon which was left beyond the scope of this paper and which, as far as we know, has not been studied neither theoretically nor experimentally. It is well-known (e.g. [3]) that the magnetic bremsstrahlung leads to the radiative self-polarization of the electron. Formally, this is due to the fact that the differential probability contains the term proportional to  $\vec{\xi} \cdot \mathbf{H}$  (here  $\mathbf{H}$  is the vector of the external magnetic field) which depends on the angle between  $\vec{\xi}$  and  $\mathbf{H}$ . A similar effect was studied in [16] in connection with the axial channeling of electrons/positrons. If one takes into account the radiative loss (which is the case when  $\chi > 1$  and  $\gamma \gg 1$ ) then there appears a strong interaction of the spin with the field of radiation,  $\mathbf{H}_r$  [4]. This results in (a) a noticeable change of the typical time  $\tau$  of the radiative self-polarization, and (b) in radiative damping which leads to the decrease of  $|\vec{\xi}|$ . Later these phenomena were considered in connection with the planar channeling of ultra-relativistic electrons/positrons in slightly bent crystals [17, 18, 19]. It was demonstrated that there appear additional terms, due to the centrifugal force in the bent channel, which influence the spin-precession, and, as a result, the time of the self-polarization. We note here that the planar channeling is more preferable than the axial one if studying the effect of radiative self-polarization. The reason is that the terms proportional to  $\vec{\xi} \mathbf{H}$  ( $\mathbf{H}$  is the effective magnetic field acting on the particle in the channel) are less influenced by the averaging over the phase distribution in the planar case.

In our mind it will be very interesting to carry out the analysis (theoretically and, if feasible, experimentally as well) of the self-polarization of a bunch of ultra-relativistic particles undergoing channeling in a crystal whose channels are periodically bent. In this case there arises very intensive radiation, additional to the well-known channeling radiation, due to the periodicity of the trajectory of the projectile [20].

## Acknowledgments

The authors are grateful to Prof. E. Uggerhøj and Dr. U. Mikkelsen for sending the manuscript of the paper [1] prior to its publication.

The research was supported by DFG, GSI, and BMFT. AVK and AVS acknowledge the support from the Alexander von Humboldt Foundation.

## References

- [1] Kirsebom K, Mikkelsen U, Uggerhøj E, Elsener K, Ballestrero S, Sona P, and Vilakazi Z Z 2001 *Phys. Rev. Lett.* **87** 054801
- [2] Berestetskii V B, Lifshitz E M, and Pitaevskii L P 1982 *Quantum Electrodynamics* (Oxford: Pergamon)
- [3] Sokolov A A and Ternov I M 1986 *Radiation from Relativistic Electrons* (New York: AIP)
- [4] Baier V N, Katkov V M and Fadin V M 1973 *Radiation from Relativistic Electrons* (Moscow: Atomizdat) (in Russian)
- [5] Baier V N, Katkov V M and Strakhovenko V M 1998 *Electromagnetic Processes at High Energies in Oriented Single Crystals* (Singapore: World Scientific)
- [6] Katkov V M and Strakhovenko V M 2001 *Zh. Eksp. Teor. Fiz.* **119** 649 (Engl. transl. *JETP* **92** 561)
- [7] Lindhard J 1991 *Phys. Rev. A* **43** 6032
- [8] Sørensen A H 1996 *Nucl. Instrum. Methods B* **119** 1
- [9] Augustin J, Schäfer A and Greiner W 1995 *Phys. Rev.* **34** 1
- [10] Lindhard J 1965 *Mat. Fys. Medd. Dan. Vid. Selsk* **34** 1
- [11] Abramowitz M and Stegun I E 1964 *Handbook of Mathematical Functions* (New York: Dover)
- [12] Gemmell D S 1974 *Rev. Mod. Phys.* **46** 129
- [13] Landau L D and Pomeranchuk I Ya 1965 *The Collected Papers of L.D.Landau* (NY: Pergamon); Migdal A B 1956 *Phys. Rev.* **103** 1811
- [14] Fomin S P, Jejcic A, Maillard J, Shul'ga N F and Silva J 1996 *Nucl. Instrum. Methods* **119** 59
- [15] Baurichter A, Kirsebom K, Kononets Yu V *et al* 1997 *Phys. Rev. Lett.* **79** 3415
- [16] Bagrov V G, Ternov I M and Kholomai B V 1984 *Sov. Phys. JETP* **59** 622 (New York: AIP)
- [17] Baryshevsky V G and Grubich 1979 *Pis'ma Zh. Tekh. Fiz.* **5** 1527 (Engl. transl. *Sov. Tech. Phys. Lett.* **5** 647)
- [18] Baryshevsky V G 1982 *Channeling, Radiation and Reactions in Crystals at High Energies* (Minsk: Buelorussian State University Press) (in Russian)
- [19] Mikhalev V L and Rzaev R A 1982 *Zh. Eksp. Teor. Fiz.* **82** 1713 (Engl. transl. *JETP* **55** 991)
- [20] Korol A V, Solov'yov A V, and Greiner W 1998 *J.Phys.G.: Nucl. Part. Phys.* **24** L45; 1999 *Int. J. Mod. Phys. E* **8** 49; 2000 *Int. J. Mod. Phys. E* **9** 77; 2001 *J.Phys.G.: Nucl. Part. Phys.* **27** 95; Krause W, Korol A V, Solov'yov A V, and Greiner W 2000 *J.Phys.G.: Nucl. Part. Phys.* **26** L87